

Swift captures the spectrally evolving prompt emission of GRB 070616[★]

R. L. C. Starling,^{1†} P. T. O’Brien,¹ R. Willingale,¹ K. L. Page,¹ J. P. Osborne,¹
M. De Pasquale,² Y. E. Nakagawa,³ N. P. M. Kuin,² K. Onda,⁴ J. P. Norris,^{5,6}
T. N. Ukwatta,^{7,8} N. Kodaka,⁴ D. N. Burrows,⁹ J. A. Kennea,⁹ M. J. Page,² M. Perri¹⁰
and C. B. Markwardt^{7,11}

¹Department of Physics and Astronomy, University of Leicester, University Road, Leicester LE1 7RH

²Mullard Space Science Laboratory, University College London, Holmbury St. Mary, Dorking, Surrey RH5 6NT

³Department of Physics and Mathematics, Aoyama Gakuin University, 5-10-1 Fuchinobe, Sagami-hara, Kanagawa 229-8558, Japan

⁴Department of Physics, Saitama University, Shimo-Okubo 255, Saitama 338-8570, Japan

⁵Denver Research Institute, University of Denver, Denver, CO 80208, USA

⁶Visiting Scholar, Stanford University, Stanford, CA 94305, USA

⁷NASA Goddard Space Flight Center, Greenbelt, MD 20771, USA

⁸Center for Nuclear Studies, Department of Physics, The George Washington University, Washington, DC 20052, USA

⁹Department of Astronomy and Astrophysics, The Pennsylvania State University, 525 Davey Lab, University Park, PA 16802, USA

¹⁰ASI Science Data Center, via Galileo Galilei, 00044 Frascati, Italy

¹¹Department of Astronomy, University of Maryland, College Park, MD 20742, USA

Accepted 2007 November 23. Received 2007 November 22; in original form 2007 October 1

ABSTRACT

The origins of gamma-ray burst (GRB) prompt emission are currently not well understood and in this context long, well-observed events are particularly important to study. We present the case of GRB 070616, analysing the exceptionally long-duration multi-peaked prompt emission, and later afterglow, captured by all the instruments on-board *Swift* and by *Suzaku* Wide-Band All-Sky Monitor (WAM). The high-energy light curve remained generally flat for several hundred seconds before going into a steep decline. Spectral evolution from hard to soft is clearly taking place throughout the prompt emission, beginning at 285 s after the trigger and extending to 1200 s. We track the movement of the spectral peak energy, whilst observing a softening of the low-energy spectral slope. The steep decline in flux may be caused by a combination of this strong spectral evolution and the curvature effect. We investigate origins for the spectral evolution, ruling out a superposition of two power laws and considering instead an additional component dominant during the late prompt emission. We also discuss origins for the early optical emission and the physics of the afterglow. The case of GRB 070616 clearly demonstrates that both broad-band coverage and good time resolution are crucial to pin down the origins of the complex prompt emission in GRBs.

Key words: gamma-rays: bursts.

1 INTRODUCTION

The prompt emission mechanism for gamma-ray bursts (GRBs) is commonly attributed to internal shocks due to collisions of shells of different Lorentz factors ejected from the vicinity of a compact

object (Rees & Mészáros 1994). Later afterglow emission comes from an external shock as the GRB blastwave decelerates through interaction with the surrounding medium (Mészáros & Rees 1997). Though the general picture appears applicable to most GRBs, the details are far from understood and other models, in particular magnetized flows, have also been proposed (e.g. Mészáros, Rees & Papatthanassiou 1994; Usov 1994; Kumar et al. 2007; Zhang 2007).

The advent of the *Swift* mission (Gehrels et al. 2004) has revealed additional features, for example steep decays and X-ray flares (Burrows et al. 2005a), whose properties are consistent with an internal origin (e.g. Tagliaferri et al. 2005; Nousek et al. 2006; O’Brien et al. 2006; Chincarini et al. 2007; Falcone et al. 2007). The steeply decaying phases that directly follow both prompt emission and

[★]This paper is dedicated to the memory of Dr Francesca Tamburelli who died during its production. Francesca played a fundamental role within the team which is in charge of the development of the *Swift* X-Ray Telescope (XRT) data analysis software at the Italian Space Agency’s Science Data Centre in Frascati. She is sadly missed.

†E-mail: rlcs1@star.le.ac.uk

X-ray flares are usually interpreted as due to the curvature effect (e.g. Kumar & Panaitescu 2000) where high latitude emission is delayed with respect to that on-axis. However, significant spectral evolution is not expected in this model, and new mechanisms must be invoked to explain those observations that do show spectral evolution during the steep decay phase (Zhang, Liang & Zhang 2007).

Of particular interest are the longest duration GRBs in which the relationship between various possible early emission components can be studied. Observationally, very few GRBs are detected in γ -rays for more than 400 s as quantified using the T_{90} parameter. For example, approximately 0.5 per cent of the BATSE (Burst and Transient Source Experiment) sample meets this criteria (Paciesas et al. 1999). Some of the very long duration GRBs include those with a precursor or a late flare (e.g. Price et al. 2002; Nicastro et al. 2004). Interestingly, the very long GRBs also include several FRED-like (fast rise, exponential decay) events which can be spectrally quite soft (Giblin et al. 1999; in't Zand et al. 2000).

In the *Swift* era it remains true that very few GRBs have a $T_{90} > 400$ s. The longest is GRB 060218, which is an unusually long, low luminosity, spectrally soft GRB (Campana et al. 2006b). In the first *Swift* Burst Alert Telescope (BAT) catalogue (Sakamoto et al. 2007) there are only three others: GRB 060929, which has a spectrally soft, late giant flare (Palmer et al. 2006); GRB 070129, for which BAT triggered on a precursor (Krimm et al. 2007); and GRB 070616.

Here we present data for the case of GRB 070616, in which the prompt emission shows a very complex multi-peaked structure, leading to one of the longest prompt emission durations ever recorded. We take advantage of extensive coverage of such a long burst by the *Swift* BAT (Barthelmy et al. 2005), the X-Ray Telescope (XRT; Burrows et al. 2005b) and the UV/Optical Telescope (UVOT; Roming et al. 2005). Combining data from *Swift* and *Suzaku* (Mitsuda et al. 2007) we study the evolution of the prompt emission spectrum, following the temporal variability of the peak energy, and study the development of the afterglow component.

In Section 2 we describe the *Swift* and *Suzaku* observations. In Section 3 we outline the X-ray and γ -ray temporal characteristics. In Section 4 we model the X-ray to γ -ray spectra and investigate spectral evolution. We discuss the discovery of an optical transient (OT) in the UVOT images in Section 5 and go on to model the spectral energy distributions (SEDs) in Section 6. In Section 7 we present possible interpretations for our findings, and discuss them in the context of the blastwave model and in comparison with other GRBs, with summary and conclusions in Section 8.

2 OBSERVATIONS

On 2007 June 16 at 16:29:33 UT (hereafter T_0), the *Swift* BAT triggered on and located GRB 070616 (trigger=282 445; Starling et al. 2007a). This was an image trigger, where the GRB is detected by forming an image from the collected counts which is then searched for a new point source. *Swift* slewed immediately to the BAT location. T_{90} (15–350 keV) is 402 ± 10 s (estimated error including systematics), which is among the longest T_{90} values for BAT GRBs.

The XRT began observing the field at 16:31:44 UT, 131 s after the BAT trigger; a bright, fading and uncatalogued X-ray source was clearly detected. XRT observed the source for a total exposure of 144.5 ks out to $T_0 + 3.7 \times 10^5$ s, beginning in windowed timing (WT) mode at $T_0 + 137$ s and continuing in photon counting (PC) mode at $T_0 + 976$ s. Using 899 s of overlapping XRT PC mode data and UVOT V-band data, we obtain an astrometrically corrected X-ray position (using the USNO-B1 catalogue; Goad et al. 2007b) of RA (J2000) = $02^h08^m36^s.59$; Dec. (J2000) = $+56^\circ56'43''.8$, with

an error of radius 2.4 arcsec (90 per cent containment). The error circle contains the bright star USNO-B1.0 1469–0076513.

The UVOT took a finding chart exposure of 100 s with the white filter starting at $T_0 + 142$ s, and continued with a long V-band exposure followed by cycling through all seven filters. The count rates in V- and U-band exposures between 250 and 1050 s after the trigger show a significant excess (at $\geq 3\sigma$) with respect to late observations (> 1 d after the trigger) at the position of the USNO-B1.0 star. We discuss this further in Section 5.

The *Suzaku* Wide-Band All-Sky Monitor (WAM; Yamaoka et al. 2005), one element of the Hard X-ray Detector (HXD; Takahashi et al. 2007) with total bandpass 50 to 5 MeV, detected GRB 070616 at 16:31:50 UT, 137 s after the *Swift* BAT trigger. The observations cover 140 s of the GRB emission, truncated by passage into the South Atlantic Anomaly. With these data alone we put a limit on the GRB duration of T_{90} of > 112 s over 150–700 keV, consistent with the BAT (15–350 keV) T_{90} .

The *Swift* data were processed with the standard *Swift* data reduction pipelines, and spectra and light curves were extracted with XSELECT. All XRT spectra are grouped such that a minimum of 20 counts lie in each bin, and X-ray light curves have a minimum of 15 source region counts per bin. We used a source extraction region of box width 40 pixel for XRT spectra in WT mode (1 pixel = 2.36 arcsec). In the first orbit of PC mode data, emission from the source was piled up, and spectra were extracted using a 20-pixel radius annulus excluding the inner 4 pixel in radius; a correction for this was made to the ancillary response file. Thereafter a circular source region of radius 17 pixel was employed. Background spectra were extracted from a nearby source-free region of radius 86 pixel. Spectral fitting was performed in XSPEC (Arnaud 1996) using version 008 response files. Errors are given at the 90 per cent confidence level throughout, unless otherwise stated.

3 TEMPORAL CHARACTERISTICS OF THE PROMPT EMISSION

Light curves for the prompt emission in all observed bands are shown in Fig. 1. The γ -ray light curves show no strongly peaked or variable emission around T_0 , as is common for BAT image triggers such as this. BAT triggered instead on a gradual rise which lasted approximately 100 s before the first and strongest peak, centred at $T_0 + 120$ s. Thereafter multiple blended peaks continue the prompt emission out to $T_0 + 500$ –600 s. At this point the γ -ray emission appears to return to the count rate at which it began at T_0 , whilst the X-ray emission begins a steep decay lasting until $T_0 + 1200$ s (Fig. 2), and the V-band optical emission continues a steady rise (Fig. 1).

The X-ray observations cover much of the time period over which BAT could detect the source, and we constructed a joint BAT–XRT light curve to compare emission from the two bands. This was done by performing joint power-law fits to fine time-sliced BAT–XRT (WT) spectra, and extrapolating the BAT spectra to the XRT energy band. The main peaks in the multi-peaked prompt emission are found to be temporally coincident, strongly suggesting that the X-ray and γ -ray emission come from the same component: the GRB prompt emission. In contrast, the V-band optical data show a slowly rising light curve from $T_0 + 250$ –1000 s which is not mimicked in any of the high-energy bands (Fig. 1).

We performed a lag analysis (e.g. Norris et al. 1996) over two intervals in the BAT light curve: ~ 70 s covering the largest peak, and ~ 155 s covering the flat multi-peaked structure following the largest peak. We use the four BAT channels 15–25 keV (channel 1),

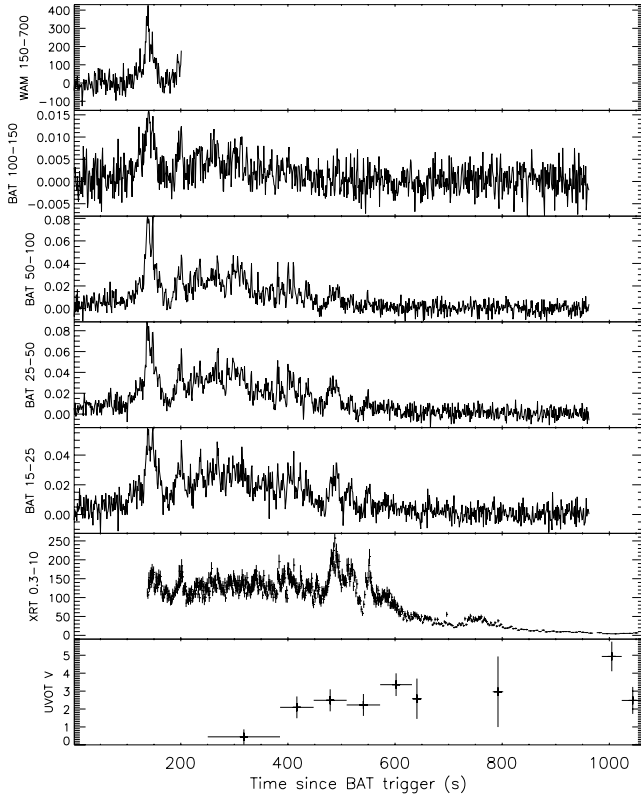


Figure 1. Light curves for the *Suzaku* WAM and all *Swift* instruments are shown in count s^{-1} . The instrument and, where appropriate, the energy range used in keV are given in the y-axis labels. We show here the WAM 1 s light curve and the mask-weighted 1 s light curves for the BAT in four individual energy ranges. The UVOT observed in all seven of its filters, but we only show the V band here (500–560 nm), in which the majority of the detections were obtained, for clarity; USNO-B1.0 1469–0076513 has been subtracted.

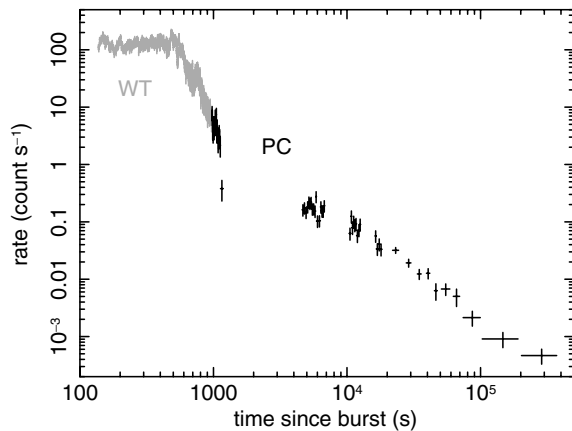


Figure 2. The XRT 0.3–10 keV count rate light curve, plotted in log space.

25–50 keV (channel 2), 50–100 keV (channel 3) and 100–350 keV (channel 4) and 256 ms time binning. For the first interval we find the following lags:

$$3 \rightarrow 1 = 220^{+90}_{-150} \text{ ms}, \quad 4 \rightarrow 2 = 410 \pm 200 \text{ ms};$$

and in the second interval the lags have decreased to

$$3 \rightarrow 1 = 64^{+64}_{-72} \text{ ms}, \quad 4 \rightarrow 2 = 0^{+80}_{-112} \text{ ms}.$$

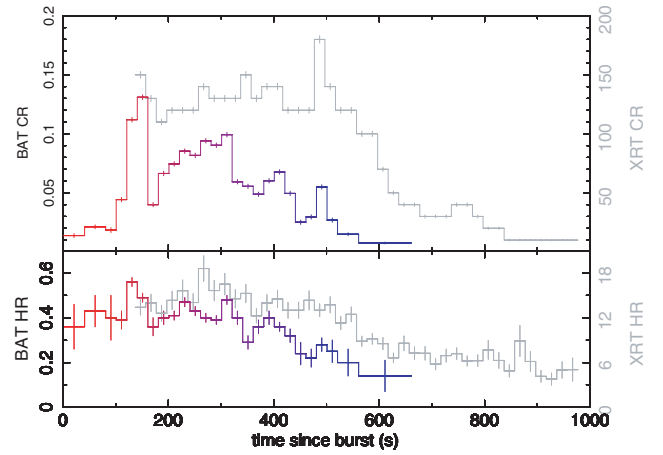


Figure 3. Count rate (CR, upper panel) and hardness ratio (HR, lower panel) against time for XRT (1–10/0.3–1 keV, 10 s bins, grey) and BAT (50–100/15–50 keV, 10, 20 or 50 s bins, colour scale).

The time resolution of the analysis prevents accurate measurements of lags < 256 ms, causing the relatively large errors reported here.

We attempted to model the underlying temporal behaviour of the prompt X-ray emission by fitting a multiply broken power-law model to the XRT light curve, as is often done for complex GRB light curves. We find the following temporal slopes, α ($F \propto t^{-\alpha}$), and break times T_{bk} : $\alpha_1 = -(0.08^{+0.03}_{-0.01})$ up to $T_{\text{bk},1} = 524^{+2}_{-3}$, $\alpha_2 = 4.87^{+0.11}_{-0.08}$ up to $T_{\text{bk},2} = 999^{+18}_{-24}$ and $\alpha_3 > 10$ up to 1200 s (the steepest segment of the decay has a slope so large when fit with a simple power law it is difficult to accurately measure). Between the steep slope and the first probable afterglow emission, $T_0 + 1130$ to $T_0 + 5800$ s, we measure $\alpha_{\text{plateau}} = 0.5^{+0.3}_{-0.2}$ using a power-law fit to the last point on the steep decay and the second orbit of PC mode data. The afterglow temporal slope from > 4600 s using this method is $\alpha_4 = 1.46 \pm 0.05$.

For the XRT and BAT we obtained hardness ratios as a function of time (Fig. 3). The BAT hardness ratio (50–100/15–50 keV) remained approximately constant until $T_0 + 285$ s when the spectra softened significantly over the remainder of the γ -ray observations. The XRT hardness ratio (1–10/0.3–1 keV) shows the same behaviour, with the spectral evolution beginning at approximately $T_0 + 500$ s (see also Fig. 10). In both bands the emission begins with a hard spectrum, evolving to become softer. The source is spectrally harder at higher count rates, as shown in Fig. 4. In the lower panel of Fig. 4 we show that flares themselves are not driving this correlation, although they are consistent with it, but that there is an overall trend in the hardness ratios with only the smaller scale changes corresponding to hardening within individual flares (individual flares can be seen as loops, following the colour scale from red through to blue which represents the passage of time).

4 SPECTRAL FITTING

4.1 X-ray

To investigate the spectral evolution seen in Figs 3 and 4, we began by characterizing the XRT X-ray spectrum for the prompt emission interval. All results are given in Table 1. To test for the presence of intrinsic absorption, we extracted a time-averaged spectrum over the time range $T_0 + 137$ –963 s. We fit the spectrum with a power-law model with absorption set initially to the Galactic value of

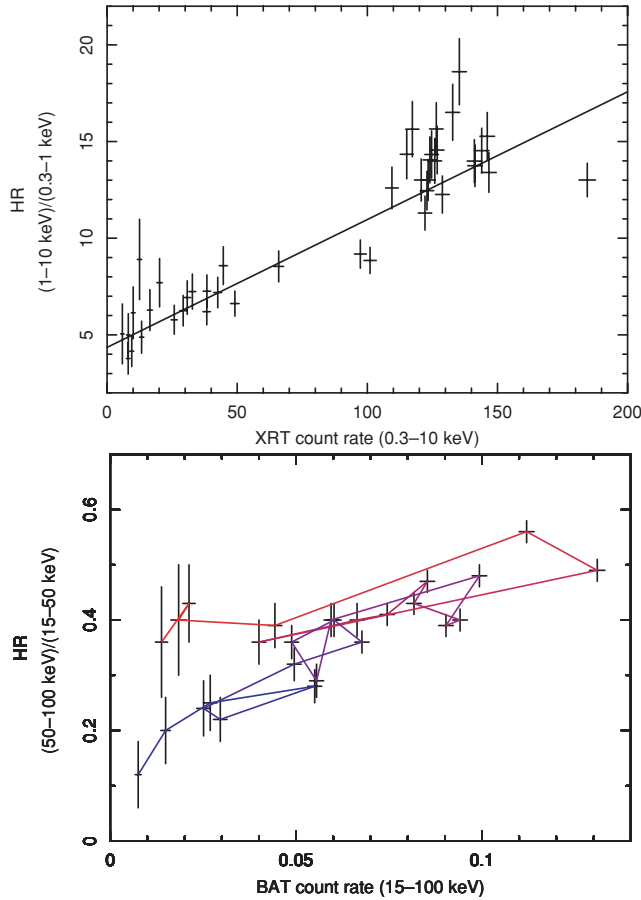


Figure 4. Hardness ratio against count rate for XRT (upper) and BAT (lower). The evolution of both quantities with time is shown by the colour gradient in the BAT panel, going from red to blue as time increases from T_0 to $T_0 + 650$ s. This colour gradient is identical to that shown in Fig. 3. The general trend of harder spectra at higher count rates is visible, and within this we see individual loops of soft–hard–soft evolution. Each loop shows the effect of the larger individual flares.

$N_{\text{H,Gal}} = 0.35 \times 10^{22} \text{ cm}^{-2}$ [LAB (Leiden/Argentine/Bonn) survey; Kalberla et al. 2005] and then allowed to go free. The inclusion of a small column of intrinsic absorption, amounting to $5 \times 10^{20} \text{ cm}^{-2}$ at $z = 0$, is required according to the F -test (F -statistic = 6×10^{-15} , Table 1).

We then extracted X-ray spectra in 100-s time bins from $T_0 + 137$ to $T_0 + 837$ s, and two further longer time bins of sizes 126 and 224 s to extend coverage to the end of the steeply decaying phase ($T_0 + 1200$ s). We fit these spectra with a power law plus Galactic+intrinsic absorption (amounting to a total column of $N_{\text{H}} = 0.4 \times 10^{22} \text{ cm}^{-2}$). We also allowed the intrinsic absorption column to vary to test for any temporal changes which may be caused by e.g. ionization by the GRB emission, but found no variation confirming that the time-averaged $N_{\text{H,intrinsic}}$ that we have applied is appropriate throughout. We observed the power-law slope to change from $\Gamma \sim 1.1$ to $\Gamma \sim 2.3$ in ~ 800 s, indicating that a spectral softening occurred in the X-ray band. This begins after the $T_0 + 337$ – 437 s segment, and corresponds to the time of the change in the X-ray hardness ratio (see Fig. 3).

We also fit a broken power-law model to the same data, initially with Galactic absorption only. The broken power-law model pro-

Table 1. X-ray spectral fits, using the XRT energy range 0.3–10 keV, and over varying time ranges covering the prompt phase: $T_0 + 137$ – 1200 s. We test the single power-law model with various absorption columns applied. F -stat refers to the F -test statistic when comparing the fits with absorbing column allowed to vary against those fixed at the Galactic column of $0.35 \times 10^{22} \text{ cm}^{-2}$.

Time (s)	$N_{\text{H}} \times 10^{22} \text{ cm}^{-2}$	Γ	$\chi^2/\text{d.o.f.}$	F -stat
137–963	0.35	1.26 ± 0.01	897/720	
137–237	0.35	1.06 ± 0.03	346/387	
237–337	0.35	$0.99^{+0.02}_{-0.03}$	398/409	
337–437	0.35	$1.13^{+0.02}_{-0.03}$	393/410	
437–537	0.35	1.30 ± 0.02	489/396	
537–637	0.35	1.59 ± 0.03	288/284	
637–737	0.35	1.84 ± 0.05	150/127	
737–837	0.35	$1.85^{+0.05}_{-0.06}$	109/111	
837–963	0.35	1.97 ± 0.10	59/51	
976–1200	0.35	2.2 ± 0.3	2.44/6	
137–963	0.40 ± 0.01	$1.34^{+0.01}_{-0.02}$	824/719	6×10^{-15}
137–237	0.39 ± 0.03	$1.09^{+0.06}_{-0.03}$	341/386	0.02
237–337	$0.42^{+0.03}_{-0.07}$	$1.07^{+0.03}_{-0.05}$	385/408	2×10^{-4}
337–437	0.42 ± 0.03	1.21 ± 0.04	375/409	1×10^{-5}
437–537	0.49 ± 0.03	$1.50^{+0.03}_{-0.05}$	397/395	1×10^{-19}
537–637	$0.42^{+0.04}_{-0.02}$	$1.71^{+0.05}_{-0.04}$	258/283	2×10^{-8}
637–737	$0.42^{+0.05}_{-0.04}$	1.96 ± 0.09	142/126	0.01
737–837	$0.39^{+0.06}_{-0.03}$	$1.91^{+0.09}_{-0.06}$	104/110	0.02
837–963	$0.30^{+0.05}_{-0.07}$	$1.86^{+0.11}_{-0.16}$	56/50	0.11
976–1200	<0.9	$2.1^{+0.7}_{-0.5}$	2.35/5	0.68
137–237	0.40	1.12 ± 0.03	341/387	
237–337	0.40	$1.05^{+0.02}_{-0.03}$	385/409	
337–437	0.40	$1.19^{+0.02}_{-0.03}$	376/410	
437–537	0.40	$1.37^{+0.03}_{-0.02}$	431/396	
537–637	0.40	$1.68^{+0.03}_{-0.04}$	261/284	
637–737	0.40	$1.93^{+0.07}_{-0.06}$	143/127	
737–837	0.40	$1.95^{+0.05}_{-0.06}$	104/111	
837–963	0.40	2.06 ± 0.10	64/51	
976–1200	0.40	2.3 ± 0.3	2.55/6	

vides statistically equal or better fits than the absorbed power-law model in most cases, but this may be a symptom of the need for intrinsic absorption, and/or possibly additional spectral curvature. Adding $5 \times 10^{20} \text{ cm}^{-2}$ of intrinsic X-ray absorption does not significantly improve the majority of the broken power-law fits. Although it is difficult to statistically distinguish between a power law plus intrinsic extinction and a broken power law, we find that the break energies and power-law slopes in the latter model move seemingly randomly in time whereas the steepening in the single power-law model matches the hardness ratio behaviour very well. In general, we expect that there will be some material within the host galaxy that lies in front of the GRB and along our line-of-sight causing detectable X-ray absorption (e.g. Campana et al. 2006a). We therefore do not consider the broken power-law model further in fits to the XRT data.

The X-ray afterglow during the second orbit of PC mode data ($T_0 + 4608$ – 6976 s) shows a soft spectrum which is well fitted by a single absorbed (Galactic+intrinsic as above) power law with

$\Gamma = 2.53^{+0.20}_{-0.19}$ ($\chi^2/\text{d.o.f.} = 11/13$). No spectral variation is seen through the afterglow phase when comparing the above time range with data from $T_0 + 10$ ks onwards which are well fit with a power law of photon index $\Gamma = 2.62^{+0.19}_{-0.17}$ ($\chi^2/\text{d.o.f.} = 14/16$).

4.2 X-ray to γ -ray

We now extend the above analysis to include the higher energy BAT spectrum. First, we extracted a time-averaged BAT–XRT spectrum covering the prompt emission phase from the start of XRT observations to the end of source visibility with the BAT (137–963 s). We fit this with three models: a power law, broken power law and the Band function (Band et al. 1993). The normalization for each instrument is always tied such that they are equal. In the Band function fits we fixed the high-energy power-law slope to $\beta = 2.36$ as found in the *Suzaku* spectrum (Morigami et al. 2007, and adopting $F_\nu \propto \nu^{-\beta}$), since the energy range with slope β is expected, at least initially, to lie above the BAT band. Each model was also absorbed by either the Galactic column alone or the previously determined Galactic+intrinsic column. Again inclusion of the small amount of intrinsic absorption improved the power-law and Band fits, but was not a significant improvement for the broken power-law fits. Results are given in Table 2. A single power law is a poor representation of the time-averaged joint spectrum, and we find the Band function or a broken power law provides a better fit.

To follow the spectral evolution, we time sliced the BAT data into six 100-s bins covering $T_0 + 137$ –737 s, corresponding to some of those extracted for the XRT. We fit the three models listed above to the joint BAT–XRT spectra for each time bin, this time absorbed by the combination of Galactic and intrinsic absorption. The single power-law model shows the same softening of the spectral slope with time as was seen for the time-sliced XRT data. The broken power law or the Band function again provides a better fit than a single power-law model. The broken power-law model fits suggest a fairly constant break in the middle of the X-ray band at ~ 4 –5 keV (we note that the fits are biased towards the X-ray band where there are the greatest number of counts). In the Band function fits the peak energy is derived from the free parameters α (low-energy power-law

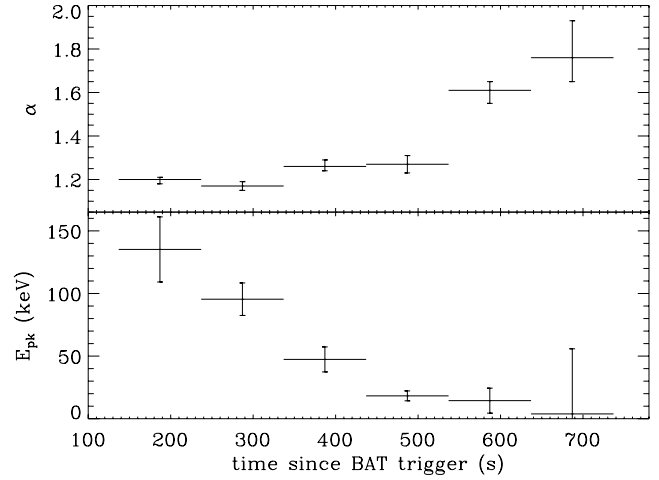


Figure 5. The Band model fitted to the BAT–XRT spectra in seven 100-s intervals, where the fitted parameters α (upper panel), and E_0 combine to give E_{pk} (lower panel). 90 per cent errors on E_{pk} have been calculated using average symmetrical error bars for α and E_0 .

index) and E_0 (characteristic energy) and the fixed parameter $\beta = 2.36$ (high-energy power-law slope) using

$$E_{\text{pk}} = E_0(2 - \alpha) \quad (1)$$

(see Band et al. 1993 for a detailed description of the Band function; errors on E_{pk} are calculated using average symmetrical error bars). E_{pk} can be well constrained and is observed to move to lower energies with time from 135 down to 4 keV in ~ 600 s (Fig. 5, Table 2), while the spectral slope α also varies gradually, softening with time.

To confirm the validity of the high-energy spectral slope we fixed in the previous Band function fits and the position of the peak energy derived from fits to the *Swift* data alone, we performed power-law fits to the *Suzaku* WAM spectrum. The constraints we derive on the power-law slopes are consistent with the value $\beta = 2.36$ used in previous analysis (see Table 2). We then performed joint fits for WAM, BAT and XRT. The results allow us to confirm the previous findings

Table 2. Joint spectral fits, using the energy ranges XRT 0.3–10 keV, BAT 15–130 keV and WAM 150–800 keV, and over varying time ranges covering $T_0 + 137$ –963 s. Three models are tested: power law, broken power law and Band function. In all Band fits $\beta = 2.36$; α , β and Γ refer to photon indices.

Time (s)	N_{H} (fixed) $\times 10^{22} \text{ cm}^{-2}$	Power law Γ	$\chi^2/\text{d.o.f.}$	Γ_1	Broken power law E_{bk} (keV)	Γ_2	$\chi^2/\text{d.o.f.}$	α	Band function E_0 (keV)	E'_{pk} (keV)	$\chi^2/\text{d.o.f.}$
BAT–XRT joint fits											
137–963	0.35	1.45 ± 0.01	2004/772	1.20 ± 0.02	4.2 ± 0.2	1.57 ± 0.01	892/770	1.30 ± 0.01	90^{+8}_{-6}	63 ± 7	1211/774
137–963	0.40	1.48 ± 0.01	1479/772	$1.31^{+0.01}_{-0.02}$	5.1 ± 0.7	1.58 ± 0.01	887/770	1.36 ± 0.01	123^{+12}_{-10}	79 ± 11	904/770
137–237	0.40	1.30 ± 0.01	602/439	$1.12^{+0.03}_{-0.02}$	$8.8^{+1.6}_{-2.6}$	$1.45^{+0.03}_{-0.05}$	413/437	$1.20^{+0.01}_{-0.02}$	169^{+29}_{-22}	135 ± 26	462/438
237–337	0.40	1.32 ± 0.01	856/461	$1.03^{+0.04}_{-0.03}$	$7.0^{+1.4}_{-0.8}$	$1.50^{+0.04}_{-0.02}$	443/459	1.17 ± 0.02	115^{+14}_{-11}	95 ± 13	561/460
337–437	0.40	1.47 ± 0.01	854/462	1.14 ± 0.03	$5.2^{+0.6}_{-0.5}$	$1.67^{+0.01}_{-0.04}$	420/460	$1.26^{+0.03}_{-0.02}$	64^{+12}_{-7}	47 ± 10	544/461
437–537	0.40	1.64 ± 0.01	886/448	$1.27^{+0.03}_{-0.05}$	$4.0^{+0.3}_{-0.4}$	$1.84^{+0.03}_{-0.02}$	455/446	1.27 ± 0.04	25^{+4}_{-3}	18 ± 4	504/447
537–637	0.40	1.80 ± 0.02	391/336	1.65 ± 0.04	5^{+8}_{-1}	$2.01^{+0.39}_{-0.05}$	317/334	$1.61^{+0.04}_{-0.06}$	37^{+9}_{-10}	14 ± 10	313/335
637–737	0.40	1.95 ± 0.05	192/179	1.88 ± 0.07	$4.3^{+1.5}_{-1.3}$	2.3 ± 0.3	184/177	$1.76^{+0.17}_{-0.11}$	16^{+94}_{-9}	4 ± 52	186/178
WAM power-law fits											
133–159	–	$2.2^{+0.3}_{-0.5}$	cstat 9.04								
WAM–BAT–XRT joint fits											
133–159	0.40	–	–	1.21 ± 0.01	246^{+60}_{-61}	$3.1^{+2.2}_{-0.9}$	146/185	$1.15^{+0.02}_{-0.01}$	419^{+88}_{-67}	356 ± 78	141/186

^aDerived parameter.

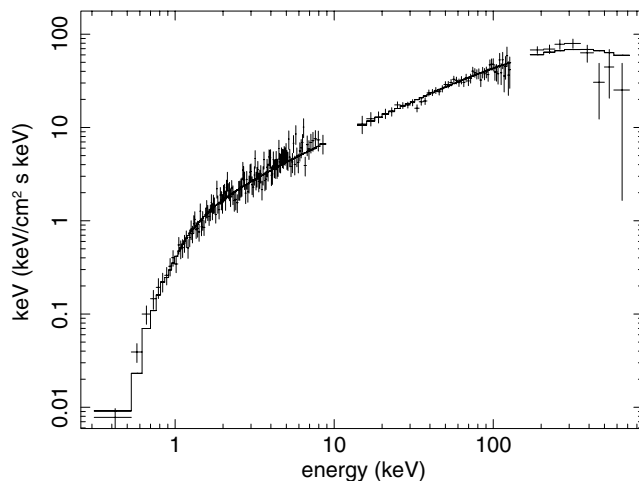


Figure 6. SED of the WAM, BAT and XRT spectra at $T_0 + 133$ – 159 s, with best-fitting absorbed Band function. The peak of the spectrum can be seen close to the boundary between the BAT and WAM bandpasses.

using a broader-band spectrum. In particular, previous BAT–XRT fits suggest the peak energy of the spectrum lies in the *Suzaku* energy band at these times (≤ 250 s) and is therefore more accurately measured in the WAM–BAT–XRT joint fit. Results are reported in Table 2. The absorbed Band function fit to the broad-band data is shown in the $E^2 F_E$ plot (energy equivalent of νF_ν) in Fig. 6.

5 IDENTIFYING THE OPTICAL AFTERGLOW

An OT was not immediately identified in the *Swift* UVOT images owing to superposition with the bright ($V = 14.4$) star USNO-B1.0 1469–0076513, whose colours are consistent with those of a hot star. The blended image of the star plus the OT is extended compared to other stars in the field. In both the UVOT V and U bands the OT was separated from the nearby star by subtracting a properly scaled later image from earlier images. For the V -band subtraction we used the sum of the first and third exposures ($T_0 + 250$ – 650 and $T_0 + 986$ – 1152 s) and a sum of two later exposures covering $T_0 + 178.2$ – 185.1 ks. The U -band subtraction used a sum of the first two exposures ($T_0 + 704$ – 723 and $T_0 + 866$ – 874 s) and a sum of three later exposures covering $T_0 + 97.2$ – 98.1 ks. The scaling was based on the total exposure times and all images were mod-8 and aspect corrected, and rebinned to 2×2 UVOT subpixels (1×1 arcsec 2). The subtracted images, of which the V band is shown in Fig. 7, reveal the sources which have varied between the considered epochs. Because of minor changes in the average point spread function (PSF) of the stellar source during the orbit, count rate noise in the original images and the combined effect of uncompensated coincidence loss where the OT and stellar PSFs overlap, the stellar image could not completely be removed and is present as a low intensity peak and ring of opposite sign. Some residual of other bright stars can thus also be found in the subtraction. The net images in the V and U filters differ slightly due to different PSF and coincidence-loss effects in each band. These complications have only a minor effect on the determination of the OT position, which is found from a combination of the subtracted images of both bands. We find a best position for the afterglow at RA (J2000) = $02^{\text{h}} 08^{\text{m}} 36.37$; Dec. (J2000) = $56^\circ 56' 44''.1$, with an uncertainty of 1.2 arcsec (radius, 90 per cent confidence). Using a 4-arcsec radius extraction region and a nearby source-free background region, we determine the count

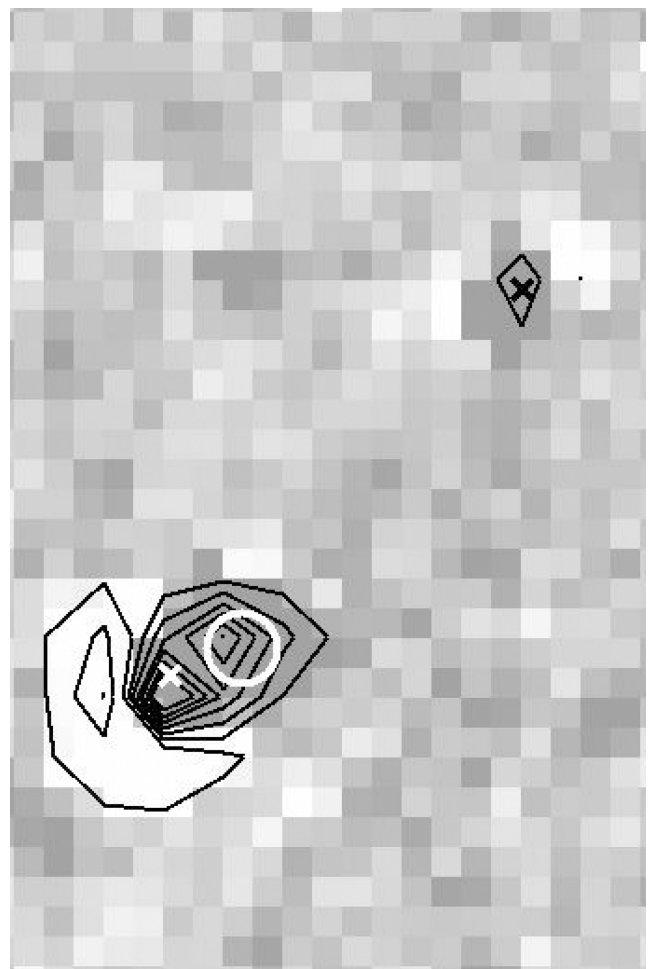


Figure 7. UVOT V -band image subtraction revealing the fading optical counterpart (negative areas are white, while positive areas are shades of grey). The white circle is the OT position and the white ‘x’ marks the centre of the star USNO-B1.0 1469–0076513, as measured from both V and U bands. Contours show both the residuals of the nearby star and the OT. The black ‘x’ indicates the position of nearby field star USNO-B1.0 1469–0076499. 1 pixel = 1 arcsec.

rates and flux densities for the OT after subtracting those of the star (Table 3). The OT is detected in the U and V bands at $>3\sigma$, and at lower significance in the B band. It is not detected in the UV filters and has disappeared below detection limits in exposures taken after 1147 s in V , 739 s in B and 870 s in U . We do not use the white filter here due to high coincidence losses. Detection of this source in the U band indicates a redshift less than ~ 3 .

A limit on the near-infrared magnitude was found using the 1.34-m ground-based TLS Tautenburg telescope using ISIS (Intermediate Dispersion Spectrograph and Imaging System) image subtraction (Alard & Lupton 1998) of two epochs, finding a conservative limit on the magnitude of $I > 19$ at 0.3 d after the trigger (K. Wiersema & D. A. Kann, private communication; see also Kann & Wilson 2007).

To support the argument that the OT is the optical counterpart to the GRB, we performed an identical analysis on another star in the same field of view. This star reveals no change of flux throughout the observations, ruling out instrumental effects as the cause of the flux variations seen in the GRB OT. Observations carried out for a further 2 d suggest the star superposed on the OT position can be

Table 3. UVOT background subtracted measurements and limits for the optical afterglow candidate, performed with a 4-arcsec aperture and with the contribution from the USNO-B1.0 star removed. All errors are 1σ and upper limits 3σ . Galactic extinction of $E(B - V) \sim 0.4$ (Schlegel et al. 1998) has not been accounted for.

Band	T_{mid}	T_{exp}	Count s $^{-1}$	Flux (μJy)
V	317.8	135	0.45 ± 0.42	113 ± 105
	416.7	62.6	2.09 ± 0.61	530 ± 154
	478.9	61.5	2.49 ± 0.61	630 ± 155
	540.9	62.4	2.23 ± 0.61	564 ± 155
	601.9	59.3	3.36 ± 0.63	850 ± 160
	640.8	18.4	2.57 ± 1.12	651 ± 284
	792.2	19.5	2.96 ± 1.97	749 ± 277
	1005	37.1	4.93 ± 0.83	1248 ± 209
	1044	41.0	2.48 ± 0.75	627 ± 191
	1085	41.1	2.45 ± 0.75	620 ± 190
	1126	41.0	2.48 ± 0.75	627 ± 191
	5942	200	<0.99	<253
	11729	885	<0.49	<124
B	734.0	10.0	3.81 ± 2.13	309 ± 173
	6044	393	<1.04	<84
	18286	615	<0.83	<67.5
U	714.0	9.8	2.74 ± 1.30	168 ± 80
	865.0	9.8	2.48 ± 1.29	152 ± 79
	5839	393	<0.86	<53
	17516	885	<0.56	<34
UVW1	765.0	39.8	<1.47	<143
UVM2	740.0	39.8	<0.84	<104
UVW2	767.5	19.0	<1.68	<139

considered a constant source, making it highly unlikely that the star in the XRT error circle flared at such time that it mimicked a GRB afterglow.

6 SPECTRAL ENERGY DISTRIBUTIONS

We constructed three optical to X-ray SEDs spanning the prompt emission phase and one SED in the afterglow phase using the ISIS spectral fitting package (Houck & Denicola 2000) and fitting in count space using the method described in Starling et al. (2007b). Throughout these fits we fixed the total X-ray absorption (Galactic+intrinsic) to the value of $N_{\text{H}} = 0.4 \times 10^{22} \text{ cm}^{-2}$ derived from the X-ray spectral fits. Galactic extinction is also included in all fits with $E(B - V) = 0.4$ (Schlegel et al. 1998). We adopt the Small Magellanic Cloud (SMC) extinction curve for fits to the intrinsic optical extinction in the host galaxy,¹ allowing for distances to the source of $z = 0-3$ (see Section 5).

The afterglow SED at 5670 s comprises UVOT *B* and *V* upper limits and XRT data. Fits to the SED are consistent with the synchrotron model, if there is a break in between the optical and X-ray

¹ The SMC extinction curve is generally a better fit to GRB host galaxy extinction than that of the Milky Way or the Large Magellanic Cloud (LMC; e.g. Schady et al. 2007; Starling et al. 2007b). The SMC has the lowest metallicity of these three nearby galaxies for which extinction curves have been derived, more closely resembling the low metallicity GRB host galaxies. We also note that solar metallicity is assumed for the X-ray absorption measurements which means the adopted $N_{\text{H, intrinsic}}$ value is likely a lower limit.

bands (discussed further in Section 7.3). Fixing the difference between the power-law slopes in this broken power-law model to 0.5, as expected for a cooling break, implies that some intrinsic absorption is also needed. Fitting to the optical upper limits and X-ray data we can set a lower limit to the required optical extinction of $E(B - V) \geq 0.1$. This amount of intrinsic optical extinction lies at the high end of the observed distribution (e.g. Starling et al. 2007b), whilst the intrinsic X-ray absorption is relatively small for a GRB (e.g. Campana et al. 2006a).

The optical emission observed at earlier times is not necessarily associated with the high-energy prompt emission. In creating the SEDs for these prompt phases we assume the optical and X-ray/ γ -ray emission do come from the same component, and determine what spectral shape and amount of intrinsic extinction would be required in this scenario. The first of the prompt phase SEDs at 284 s includes UVOT *V* band, XRT and BAT data. We fit a Band function to the spectrum with the high-energy photon index β fixed to 2.36. The availability of optical and high-energy data provides a rare opportunity for Band function fits to a broad-band SED. The *V* band data point lies below the best possible fit to the whole SED. To obtain an acceptable fit either intrinsic extinction would have to be present at the level of $E(B - V) \geq 0.05$ or both extinction and a further spectral break could be present.

The second epoch SED at 770 s includes UVOT *U* and *V* band and XRT data. We fit an absorbed power law to the spectrum. The power-law model overpredicts the optical data, illustrated in Fig. 8, and allowing for some intrinsic extinction decreases the χ^2_{reduced} value by ~ 50 per cent. In order to obtain an acceptable fit either intrinsic extinction would have to be present at the level of $E(B - V) = 0.03-1.40$ or we have a spectral break plus extinction. For the latter model we find a best fitting break energy of $0.7 \pm 0.2 \text{ keV}$, $\Gamma_1 = 1.4^{+0.3}_{-0.2}$, $\Gamma_2 = 1.97 \pm 0.05$ consistent with BAT-XRT Band function fits (Section 4.2) and $E(B - V) \leq 0.5$. The power-law slopes differ by ~ 0.5 consistent with a cooling break inferring that the cooling break moves to lower energies with time. Both single and broken power-law fits are, however, statistically acceptable and indistinguishable.

The third epoch SED at 1082 s is the least constrained: this SED covers the final part of the steep X-ray decay phase of the light curve where the X-ray source has become fainter and XRT was operating

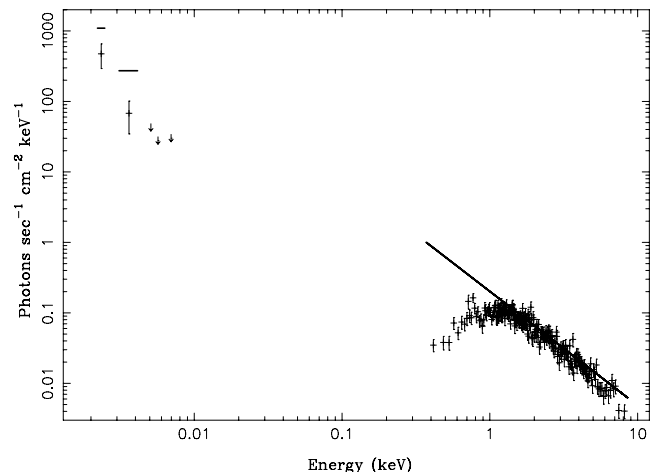


Figure 8. The SED at 770 s after the trigger: XRT and *V*- and *U*-band data and *UV* filter upper limits. The unfolded (unabsorbed) model shown as a solid line is a power-law fit to the observed *V*, *U* and X-ray data, showing the overprediction of the low-energy spectrum.

in PC mode. A joint fit of the UVOT V band data and the X-ray spectrum manages to accommodate the single optical point without inclusion of any intrinsic extinction, with a slope of $\Gamma = 1.76^{+0.05}_{-0.07}$ and $\chi^2/\text{d.o.f.} = 8.6/7$, but is inconsistent with the fit to the X-ray data alone of $\Gamma = 2.3 \pm 0.3$ (Table 1, Section 4.1) and with the afterglow SED fits. Including an intrinsic extinction component the power-law photon index is then best fit with $\Gamma = 2.3 \pm 0.3$ and the range of allowed extinction values is $E(B - V) = 0.5\text{--}2.2$. More complex models cannot be tested with this data set.

7 DISCUSSION

In GRB 070616 we have the rare opportunity to track the detailed spectral and temporal evolution from γ -rays to X-rays throughout the entire prompt emission phase. Hence we devote the majority of this discussion to the possible origins of the complex prompt emission, as well as the early optical emission, using the observational results given above. We also provide a brief discussion of the afterglow characteristics in the framework of the standard synchrotron model.

7.1 The prompt emission mechanisms

The prompt emission of GRB 070616 is atypical of GRBs in that the emission rises relatively slowly over about 100 s to a peak, then persists at a fairly constant level for 150 s in γ -rays and 350 s in X-rays before showing a rapid decline. Throughout the constant phase the light curve resembles a large number of flares or flickering superimposed on an underlying constant intensity emission. During this prompt phase we observe strong spectral evolution from hard to soft. The spectral evolution begins at $T_0 + 285$ s at γ -ray energies, while the X-ray flux is still at an approximately constant level, and begins 200 s later at X-ray energies around the onset of the steep X-ray decay (Fig. 3).

The spectral variability suggests a peak moving through the bandpass. We find that the peak of the spectrum can be accurately measured by adding the higher energy *Suzaku* WAM data to the *Swift* coverage. Assuming the Band function to model the spectrum, the spectral peak started out at the high-energy end of the BAT range – and was probably above 200 keV before the XRT or *Suzaku* observations began – and moved to lower energies to most probably lie within the XRT bandpass beyond $T_0 + 700$ s (Fig. 5). Indeed such strong spectral evolution may help explain some of the steep X-ray decline. We also find that the BAT spectral lags decreased during the prompt emission from the first main peak to ~ 200 s later: such lag evolution appears to be common among spectrally evolving GRBs (Cannizzo et al., in preparation). The second, lower lag measurement was taken just after the BAT hardness ratio had begun its decrease and the spectral peak energy had fallen below 100 keV to be clearly detectable within the BAT energy range.

While the spectral peak is moving we also measure a softening of the spectrum at frequencies below the peak. The spectral index above the peak energy, β , is found to be 2.36 from the *Suzaku* data (Morigami et al. 2007). The spectrum is observed to be harder at higher count rates, as has been shown for several other GRBs (e.g. GRB 051117a, Goad et al. 2007a; GRB 061121, Page et al. 2007). Superimposed on this general trend is a hardening during the rise of individual flares, but this effect is not driving the overall evolution (Fig. 4).

Spectral evolution through the prompt phase has been noted previously, and is inconsistent with the idea that the curvature effect alone – the delayed arrival of emission from progressively higher

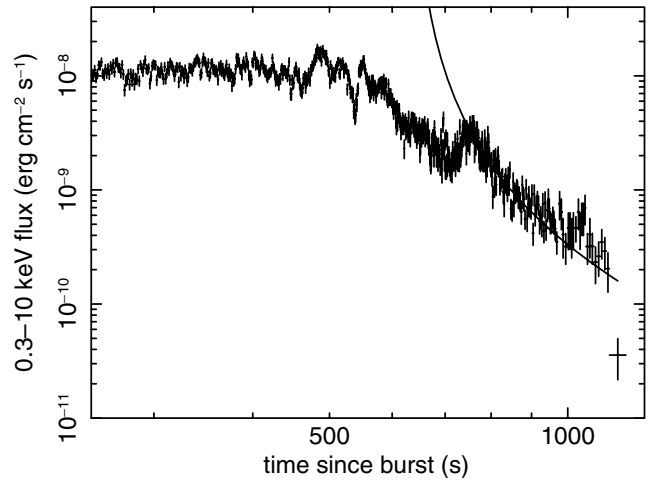


Figure 9. The XRT light curve and fit to the energy injection time for the last occurring X-ray flare using the curvature model. A variable count rate to flux conversion was applied. This fit gives a $T_{0,\text{flare}}$ of 632^{+11}_{-12} s.

latitudes within the jet – is driving the emission during the steep decay phase (e.g. Liang et al. 2006). If we try to force a curvature effect model to explain the observed steep X-ray slope from the peak of the last flare at $T_0 + 757$ s out to $T_0 + 950$ s, we would expect that phase to begin at $T_0 + 632^{+11}_{-12}$ s given the requirement of the model that $\alpha = 2 + \beta(F_\nu \propto t^{-\alpha} \nu^{-\beta})$ and adopting the average spectral energy index over that time interval of $\beta = 1.06$, Fig. 9). This would require a long initial emission period of over 600 s. In the sample of *Swift* GRBs studied by Liang et al. (2006), the typical injection of energy tends to occur at the onset of the previous large peak. The curvature effect clearly cannot explain the steepest part of the X-ray decay from $T_0 + 976\text{--}1200$ s (see last point in Fig. 9, also seen in e.g. GRB 051117a, Goad et al. 2007a; GRB 070110, Troja et al. 2007). However, the combination of the curvature effect and the strong spectral evolution we observe, which is a continuous process starting well before 600 s, may be able to account for the steep X-ray decay.

Zhang et al. (2007) studied the X-ray tails of the prompt emission for a sample of *Swift* GRBs and found that only 25 per cent of those could be fit with the curvature effect alone; those not well fit showed spectral evolution. From fits to 16 GRBs, they tested and subsequently disfavoured two possible causes of the spectrally evolving X-ray tails, namely an angle-dependent spectral index in structured jets and a superposition of the curvature effect and a power-law decay component. The observed spectral softening could, they suggest, be caused by cooling of the plasma where the cooling frequency decreases with time. This manifests itself as a cut-off power-law shape with the cut-off moving to lower energies with time, shown to be a good fit to GRB 060218 and proposed earlier for GRB 980923 (Giblin et al. 1999), and similar to our Band function results for GRB 070616. In this scenario the peak energy we track through the BAT band would be the cooling frequency. The prompt emission SED at 770 s after the trigger, including optical emission, is consistent with an absorbed broken power law where the break shows the characteristics of a cooling break (though a single absorbed power law provides an equally good fit). In the afterglow SED we most probably do detect the cooling break, hence we may have observed it moving to lower energies with time. However, we also observe softening of the low-energy power-law slope in addition to movement of a peak or cooling frequency. Other models for the

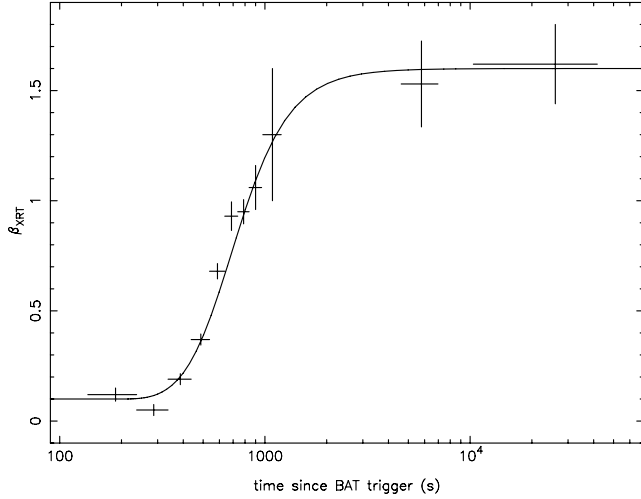


Figure 10. Spectral evolution in the XRT band, plotted as β versus time for a direct comparison with Zhang et al. (2007), where β is the power-law energy index of a single power-law fit to the XRT spectra. We model this with the curvature model plus an underlying afterglow component to the strong spectral evolution (solid line).

prompt emission have been suggested – see Zhang (2007) for a review.

We now investigate origins for the apparent spectral evolution in the simple superposition of multiple components. Fig. 10 shows the spectral evolution in the XRT band, characterized by the fitted power-law slope β ($\beta = \Gamma - 1$), displaying a similar behaviour to many of the bursts studied by Zhang et al. (2007) and resembling most closely that of GRB 060510B which also had a lengthy prompt emission duration of $T_{90} = 275$ s with some flaring (Barthelmy et al. 2006). To approximate the shape of the spectral evolution of GRB 070616 in the X-ray band (β versus time) we fit a model with two power laws:

$$F_E = A_1 t^{-\alpha_1} E^{-\beta_1} + A_2 t^{-\alpha_2} E^{-\beta_2}, \quad (2)$$

where t is time since a fitted $T_{0,\text{fit}}$ value and E is the photon energy. We fixed the spectral slopes to those of the typical measured prompt and afterglow values, $\beta_1 = 0.1$ and $\beta_2 = 1.6$. We fixed α_2 at the probable afterglow temporal slope during the plateau of 0.5 (see Section 3) while α_1 , $T_{0,\text{fit}}$ and the relative contributions of the prompt and afterglow components were left to vary. This double power-law model, overlaid on the evolution of β in Fig. 10, appears to be a reasonable description of the behaviour through the steep decay and afterglow phases, with $\alpha_1 = 3.0$, $T_{0,\text{fit}} = T_0 + 200$ s and the two components contributing equally to the flux at $T_0 + 800$ s. The spectral shape evolves due to the increasing contribution from the afterglow to the overall spectrum. We then returned to the high-energy light curve to test the double power-law model fitted above. The dashed line in the lower panel of Fig. 11 shows the double power-law model applied to the high-energy light curve. Clearly, although the evolution of β is well modelled the flux is not. We can therefore rule out a *spectrally invariant* double power-law model.

It is possible that there is a further emission component, in addition to the high-latitude emission, contributing to the steep decay ending the prompt emission, which becomes prominent between the prompt and early afterglow phases. To examine this possibility we applied the modelling procedure of O’Brien et al. (2006) and Willingale et al. (2007) in which it was shown that GRB early light curves can be well modelled by up to two emission components

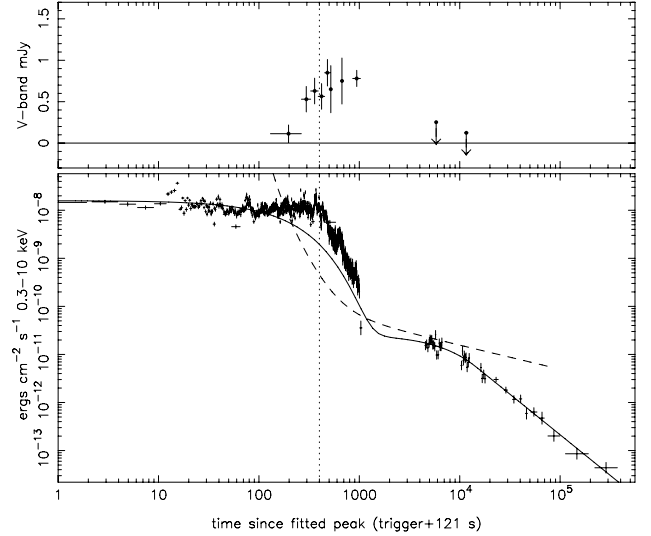


Figure 11. Top panel: UVOT V-band flux light curve. Lower panel: BAT–XRT light curve with two-component model fit following Willingale et al. (2007, solid line). This two-component model has proven a good fit to the majority of *Swift* high-energy light curves, but is unable to fit all the prompt emission of GRB 070616. The dashed line shows the flux profile from the double power-law model equation (2) used to fit the β profile (Fig. 10). This model also cannot fit the observed light curve.

Table 4. A two-component fit to the BAT–XRT light curve following Willingale et al. (2007). The trigger time has been rescaled to $T_0 + 121$ s. Quantities α_p and T_p refer to the prompt component power-law decay slope and start of that decay, respectively, and α_a and T_a refer to the afterglow component, relative to the new zero time.

Component	Parameter	Value
1	α_p	$7.37^{+0.12}_{-0.27}$
1	T_p	1400^{+214}_{-156} s
2	α_a	$1.69^{+0.23}_{-0.20}$
2	T_a	14380^{+5740}_{-4580} s

each consisting of an exponential followed by a power-law decay. The first component models the prompt emission, adjusting the zero time, T_0 , to provide the best fit. For GRB 070616 this moves zero close to the brightest peak in the prompt light curve at 121 s after the trigger. The best-fitting model to the *Swift* BAT and XRT data is given in Table 4 and Fig. 11.

We find that the light curve of GRB 070616 is not well fitted by the usual two components consisting of an exponential plus a power law decline. The first, prompt component can fit the initial prompt data following the brightest peak, but then declines until the second, afterglow component starts to dominate. This final component can be fit with a power law of slope $\alpha \sim 1.7$ from 4600 s onwards, typical of a post-plateau GRB afterglow (Table 4). There remains an excess flux dominating from some 200 to 1000 s post-trigger. We speculate that this flux plus the spectral evolution indicate an additional source of prompt emission which does not dominate in the majority of GRBs.

Interestingly, several, although not all, of the GRBs with strong spectral evolution studied in Zhang et al. (2007) are also not well fitted by the two-component light-curve model (e.g. GRB 051227 and

060614; see Willingale et al. 2007). Others not well fitted by this modelling procedure, such as GRB 051117A (Goad et al. 2007a) were identified by Zhang et al. (2007) as having evolution which they attributed to flares. Such GRBs may instead be more similar to GRB 070616. GRB 051117A, for example, shows a long, bright, slowly declining prompt emission period with flaring followed by a sharp drop to a plateau or afterglow phase. GRB 070616 may be a case where the flux remains fairly constant, with flaring, up to the sharp drop. Among the *Swift* BAT bursts we notice of order 10 bursts with an initially flat high-energy light curve, most prominent in GRB 070616, which when studied as a sample may provide more evidence in support of either a long-duration central engine or an additional component (Lyons et al., in preparation).

7.2 The origin of the early optical emission

The *Swift* era has provided a wealth of information on the early γ -ray and X-ray emission. The prompt optical emission has been harder to reveal as in most GRBs the flux level lies below that accessible to fast-response, modest aperture telescopes. Even so, for those GRBs which have been detected the relationship between the optical and X-ray emission is complex. In a very small number of cases the optical actually lies above the extrapolation of the higher energy emission (e.g. GRB 990123; Akerlof et al. 1999). The optical can be dominated by a component related to the prompt high-energy emission (e.g. Vestrand et al. 2005; Yost et al. 2007a). More usually, the optical lies below such an extrapolation, as shown for a sample of Robotic Optical Transient Search Experiment (ROTSE)-detected *Swift* GRBs by Yost et al. (2007b, using BAT data only for the extrapolations). This pattern of diverse behaviour strongly suggests a mixture of components can contribute to the prompt optical emission, including the afterglow (due to the external shock) and emission from the prompt fireball (which may include a reverse shock). In the latter case the optical should connect, possibly with a spectral break, with the prompt γ -ray–X-ray spectrum.

Few optical data sets have sufficient broad-band data to check for consistency in spectral shape as well as overall flux level, limiting our ability to constrain reddening effects as opposed to spectral breaks. For GRB 070616 the combination of long-duration prompt emission plus early optical multicolour data can provide some constraints on the relationship between the optical emission and the high-energy prompt emission. The V-band light curve shows a rise to a plateau-like phase from the first observation beginning at $T_0 + 250$ s and extending to $T_0 + 1000$ s. The optical decay does not follow the steeply decaying X-ray and γ -ray prompt emission. A gradual rise would be typical of the start of afterglow emission, seen in a number of bursts (Molinari et al. 2007). We performed a power-law fit to the V-band light curve shown in Fig. 1 and measure $\alpha = -(0.7 \pm 0.3)$. This is consistent with predictions for the afterglow rise in the fireball model of $\alpha = -0.5$ (e.g. Zhang & Mészáros 2004). Fits to the three prompt emission SEDs for GRB 070616 all show that extrapolation of the high-energy spectrum to lower energies overpredicts the optical flux; however, this may be overcome with a relatively large amount of intrinsic extinction or a combination of extinction and a spectral break, if the optical data are assumed to be prompt emission dominated.

We can compare this burst with other GRBs for which well-time-resolved prompt optical data are available, and whose light curves are not afterglow dominated from early times. For GRB 050820A, Vestrand et al. (2006) find a rising optical component plus a component correlated with the γ -ray emission. In GRB 050904 the optical data rose to a plateau before mimicking a flare seen in the X-rays

(Boër et al. 2006). Similarly in GRB 051111, Yost et al. (2007a) suggest a combination of components produce the prompt optical emission with a significant contribution to the early optical flux from an extension of the higher energy spectrum. These are similar to the case of GRB 061121 (Page et al. 2007) where the high-energy prompt emission consisted of a single large peak, which was mimicked in the optical data, although an additional spectrally evolving optical component is also seen. Extrapolation of the high-energy spectrum in GRB 061121 overpredicts the early optical emission, suggesting a spectral break. We note that the extrapolation of the high-energy spectrum to the optical band predicts a relatively higher optical flux in GRB 061121 than in GRB 070616, due to its softer high-energy spectrum.

For GRB 070616 we conclude that strong optical emission associated with the prompt phase and described by a simple extrapolation of the observed higher energy spectrum cannot be present without invoking a further spectral break in between optical and X-rays or extinction in the host at the highest end of the currently observed values (e.g. Schady et al. 2007; Starling et al. 2007b). We can likely rule out the ‘external–external’ shock model (Mészáros & Rees 1993), which requires that the broad-band prompt emission is produced by one and the same mechanism and any variability is caused by density enhancements in the external medium, given the very different behaviour of the optical and X-ray light curves.

7.3 The afterglow

After $T_0 + 4000$ s the X-ray afterglow can be considered ‘typical’ of what we know for GRB afterglows: the spectral and temporal parameters lie within the range of the ~ 250 *Swift*-observed GRBs. We test these parameters against the synchrotron model, using the closure relations for the case of a cooling break in between the optical and X-ray bands, $\nu_c < \nu_X$ and $\alpha = (3\Gamma - 4)/2$, and find that the observed temporal and spectral X-ray slopes are just consistent at the 90 per cent level and therefore follow the expectations for synchrotron emission (in the slow cooling regime). This result also indicates that the afterglow has not reached the ‘jet’ phase, in agreement with the lack of evidence for a jet break during the *Swift* observations. We do not find good agreement if the cooling frequency were to lie above the X-ray band, $\nu_c > \nu_X$, at this time, consistent with the requirement of a broken power law to best describe the SED of the late-time afterglow spectrum plus optical upper limits. Therefore, we conclude that the observed spectral break is due to the cooling frequency. The cooling frequency is likely to lie at or above the X-ray frequencies at earlier times (< 4000 s), depending on the circumburst medium density structure, but we cannot confirm this since the initial X-ray emission is prompt dominated.

We find a 90 per cent confidence range for the injected electron energy index, p , of 2.68–3.46, as determined from the measured X-ray spectral index where $\Gamma = (p + 2)/2$. This is higher than the commonly quoted ‘universal’ value of $p = 2.2$ derived from some numerical simulations of particle acceleration in relativistic shocks (e.g. Achterberg et al. 2001), but other numerical simulations (e.g. Baring 2004) and recently published observational studies of samples of afterglows (Shen, Kumar & Robinson 2006; Starling et al. 2008) find a range of allowed values for p which encompass the values we report for GRB 070616.

8 CONCLUSIONS

GRB 070616 has afforded us the rare opportunity to track the detailed spectral and temporal evolution from γ -ray to optical

wavelengths throughout much of the prompt emission phase, owing to *Swift*'s fast slew capability, the broad-band coverage provided by the combination of *Swift* with *Suzaku* WAM and the long prompt emission duration. The high-energy light curve remains generally flat for several hundred seconds before going into a steep decline.

Spectral evolution from hard to soft is clearly taking place through the prompt emission (flat and decaying phases) of GRB 070616, beginning at 285 s out to at least 1000 s. The high-energy spectrum from 0.3 to 800 keV is well modelled by a Band function. We track the spectral peak energy moving from 135 down to ~ 4 keV and measure a softening of the low-energy spectral slope from $\Gamma \sim 1.1$ to 2.3. The curvature effect, whilst contributing to the spectral shape, is not dominating during the steep decay at ~ 1000 s.

The presence of an additional component, perhaps not present in most GRBs, is favoured by the inability of a two-component fit to model the light curve. This unusual light-curve shape of an initial constant flux followed by a sharp drop, plus the strong spectral evolution, is most prominent in GRB 070616, but we note a similar structure can be found in a small number of other GRBs which are also not dominated by the curvature effect and not well fit by the two-component model.

We find that the optical data during the prompt phase are not consistent with a simple extrapolation of the high-energy spectrum, requiring either significant intrinsic extinction or some extinction plus a break in the spectrum between the X-ray and optical bands.

The afterglow is consistent with the synchrotron model, with the cooling break lying in between optical and X-ray bands at a few thousand seconds after the trigger.

The prompt emission of GRB 070616 comprises a component well fitted with a Band function and a possible further component. It is clear that both broad-band coverage and good time resolution are crucial to pinning down the origins of the complex prompt emission in GRBs.

ACKNOWLEDGMENTS

We thank E. Rol, O. Godet, P. A. Evans, G. Sato, S. T. Holland, F. E. Marshall, S. R. Oates and A. de Ugarte Postigo for useful discussions. We thank all the *Suzaku* WAM team for their contributions, in particular M. S. Tashiro, K. Yamaoka, K. Morigami and M. Ohno, and we acknowledge the whole *Swift* team for their many contributions. We thank B. Gendre for useful comments on the manuscript. RLCS, KLP and JPO acknowledge financial support from STFC.

REFERENCES

Achterberg A., Gallant Y. A., Kirk J. G., Guthmann A. W., 2001, *MNRAS*, 328, 393
 Akerlof C. et al., 1999, *Nat*, 398, 400
 Alard C., Lupton R. H., 1998, *ApJ*, 503, 325
 Arnaud K., 1996, in Jacoby G. H., Barnes J., eds, *ASP Conf. Ser. Vol. 101, Astronomical Data Analysis Software and Systems V*. Astron. Soc. Pac., San Francisco, p. 17
 Band D. et al., 1993, *ApJ*, 413, 281
 Baring M. G., 2004, *Nucl. Phys. B Proc. Suppl.*, 136, 198
 Barthelmy S. et al., 2005, *Space Sci. Rev.*, 120, 143
 Barthelmy S. et al., 2006, *GCN Circ.*, 5107
 Boër M., Atteia J. L., Damerdjy Y., Gendre B., Klotz A., Stratta G., 2006, *ApJ*, 638, L71
 Burrows D. N. et al., 2005a, *Sci*, 309, 1833
 Burrows D. N. et al., 2005b, *Space Sci. Rev.*, 120, 165
 Campana S. et al., 2006a, *A&A*, 449, 61
 Campana S. et al., 2006b, *Nat*, 442, 1008

Chincarini G. et al., 2007, *ApJ*, in press, preprint (astro-ph/0702371)
 Falcone A. D. et al., 2007, *ApJ*, in press, preprint (arXiv:0706.1564)
 Gehrels N. et al., 2004, *ApJ*, 611, 1005
 Gehrels N. et al., 2005, *Nat*, 437, 851
 Giblin T. W., van Paradijs J., Kouveliotou C., Connaughton V., Wijers R. A. M. J., Briggs M. S., Preece R. D., Fishman G. J., 1999, *ApJ*, 524, L47
 Giblin T. W., Connaughton V., van Paradijs J., Preece R. D., Briggs M. S., Kouveliotou C., Wijers R. A. M. J., Fishman G. J., 2002, *ApJ*, 570, 573
 Goad M. R. et al., 2007a, *A&A*, 468, 103
 Goad M. R. et al., 2007b, *A&A*, 476, 1401
 Houck J. C., Denicola L. A., 2000, in Manset N., Veillet C., Crabtree D., eds, *ASP Conf. Ser. Vol. 216, Astronomical Data Analysis Software Systems IX*. Astron. Soc. Pac., San Francisco, p. 591
 in't Zand J. J. M. et al., 2004, in Feroci M., Frontera F., Masetti N., Piro L., eds, *ASP Conf. Ser. Vol. 312, Third Rome Workshop on Gamma-Ray Bursts in the Afterglow Era*. Astron. Soc. Pac., San Francisco, p. 18
 Kalberla P. M. W., Burton W. B., Hartmann D., Arnal E. M., Bajaja E., Morras R., Poppel W. G. L., 2005, *A&A*, 440, 775
 Kann D. A., Wilson A. C., 2007, *GCN Circ.*, 6629
 Krimm H. et al., 2007, *GCN Circ.*, 6058
 Kumar P., Panaitescu A., 2000, *ApJ*, 541, L51
 Kumar P. et al., 2007, *MNRAS*, 376, L57
 Liang E. W. et al., 2006, *ApJ*, 646, 351
 Mészáros P., Rees M. J., 1993, *ApJ*, 405, 278
 Mészáros P., Rees M. J., 1997, *ApJ*, 476, 232
 Mészáros P., Rees M. J., Papathanassiou H., 1994, *ApJ*, 432, 181
 Mitsuda K. et al., 2007, *PASJ*, 59, S1
 Molinari E. et al., 2007, *A&A*, 469, L13
 Morigami K. et al., 2007, *GCN Circ.*, 6578
 Nicastro L. et al., 2004, *A&A*, 427, 445
 Norris J. P., Nemiroff R. J., Bonnell J. T., Scargle J. D., Kouveliotou C., Paciesas W. S., Meegan C. A., Fishman G. J., 1996, *ApJ*, 459, 393
 Nousek J. et al., 2006, *ApJ*, 642, 389
 O'Brien P. T. et al., 2006, *ApJ*, 647, 1213
 Paciesas W. S. et al., 1999, *ApJS*, 122, 465
 Page K. L. et al., 2007, *ApJ*, 663, 1125
 Palmer D., Sato G., Barthelmy S. D., Sakamoto T., Markwardt C., Gehrels N., 2006, *GCN Circ.*, 5662
 Price P. A. et al., 2002, *ApJ*, 573, 85
 Rees M. J., Mészáros P., 1994, *ApJ*, 430, L93
 Roming P. W. A. et al., 2005, *Space Sci. Rev.*, 120, 95
 Sakamoto T. et al., 2007, *ApJS*, in press, preprint (arXiv:0707.4626)
 Schady P. et al., 2007, *MNRAS*, 377, 273
 Schlegel D. J., Finkbeiner D. P., Davis M., 1998, *ApJ*, 500, 525
 Shen R., Kumar P., Robinson E. L., 2006, *MNRAS*, 371, 1441
 Starling R. L. C. et al., 2007a, *GCN Circ.*, 6542
 Starling R. L. C., Wijers R. A. M. J., Wiersema K., Rol E., Curran P. A., Kouveliotou C., van der Horst A. J., Heemsckerk M. H. M., 2007b, *ApJ*, 661, 787
 Starling R. L. C., van der Horst A. J., Rol E., Wijers R. A. M. J., Kouveliotou C., Wiersema K., Curran P. A., Weltevrede P., 2008, *ApJ*, 672, 433
 Tagliaferri G. et al., 2005, *Nat*, 436, 985
 Takahashi T. et al., 2007, *PASJ*, 59, 35
 Troja E. et al., 2007, *ApJ*, 665, 599
 Usov V. V., 1994, *MNRAS*, 267, 1035
 Vestrand W. T. et al., 2005, *Nat*, 435, 178
 Vestrand W. T. et al., 2006, *Nat*, 442, 172
 Willingale R. et al., 2007, *ApJ*, 662, 1093
 Yamaoka K. et al., 2005, *IEEE Trans. Nucl. Sci.*, 52, 2765
 Yost S. A. et al., 2007a, *ApJ*, 657, 925
 Yost S. A. et al., 2007b, *ApJ*, 669, 1107
 Zhang B., 2007, *Chin. J. Astrophys.*, 7, 1
 Zhang B., Mészáros P., 2004, *Int. J. Mod. Phys. A*, 19, 2385
 Zhang B.-B., Liang E.-W., Zhang B., 2007, *ApJ*, 666, 1002

This paper has been typeset from a \LaTeX file prepared by the author.